

Highly Elastic and Conductive Human-Based Protein Hybrid Hydrogels

Nasim Annabi, Su Ryon Shin, Ali Tamayol, Mario Miscuglio, Mohsen Afshar Bakooshli, Alexander Assmann, Pooria Mostafalu, Jeong-Yun Sun, Suzanne Mithieux, Louis Cheung, Xiaowu (Shirley) Tang, Anthony S. Weiss, and Ali Khademhosseini*

Elastomers are key components of many natural systems including organisms' organs. In addition, elastomeric polymer-based materials have been used for various applications such as tissue engineering scaffolds,^[1,2] drug delivery vehicles,^[3] models for biological studies,^[4] and substrates for engineering flexible electronics,^[5] actuators,^[6] and sensors.^[7] Although synthetic elastomers such as poly(glycerol sebacate) (PGS)^[1] and polyurethanes (PU)^[8] are stretchable and tough, they lack the bioactivity of natural elastomers. A key component of the native extracellular matrix (ECM) in elastic tissues is elastin. Thus, many researchers have tried to create biomimetic elastin-based elastomers for applications that require matrix bioactivity and elasticity. For example, naturally derived elastomeric hydrogels such as elastin-like polypeptide (ELP) gels,^[9] chemically crosslinked tropoelastin gels,^[10] photocrosslinkable tropoelastin gels,^[11,12] and animal derived elastin gels^[13,14] have been developed for biomedical applications. Although these biomimetic materials are highly elastic, their low toughness makes them unsuitable for many tissue engineering and regenerative medicine applications. Thus, several research groups have attempted to combine natural and synthetic materials to form composite elastomers with high

extensibility and toughness such as nanocomposite hydrogels,^[15] polyrotaxane gels,^[16] double network (DN) gels,^[17] hydrophobic bilayers (PDGI)/polyacrylamide (PAAm),^[18] and PAAm/alginate composite gels.^[19] The limitations of these systems include their permanent deformation, cytotoxicity, and harsh fabrication processes. These characteristics can limit their applicability for biological applications.

The aim of this study is to engineer a biocompatible and stretchable hydrogel with tunable mechanical, electrical, and biological properties based on recombinant human tropoelastin and graphene oxide (GO) nanoparticles. Tropoelastin is the dominant physiological component of elastin, where upon crosslinking it conveys both elasticity and biological activity.^[20] Tropoelastin has been used in different forms in various biomedical applications. For example, the methacryloyl-substituted tropoelastin (MeTro) has been developed as a photocrosslinkable elastomer with excellent biocompatibility^[11,12] and remarkable extensibility up to 400%.^[12] However, the elastic modulus of MeTro is limited to the range of 2.8–14.8 kPa. In addition, similar to the majority of hydrogels and polymeric elastomers, MeTro is electrically nonconductive.

Prof. N. Annabi, Dr. S. R. Shin, Dr. A. Tamayol,
M. Miscuglio, M. A. Bakooshli, Dr. A. Assmann,
Dr. P. Mostafalu, Prof. A. Khademhosseini
Biomaterials Innovation Research Center
Department of Medicine
Brigham and Women's Hospital
Harvard Medical School
Cambridge, MA 02139, USA
E-mail: alik@rics.bwh.harvard.edu

Prof. N. Annabi, Dr. S. R. Shin, Dr. A. Tamayol, M. Miscuglio,
M. A. Bakooshli, Dr. A. Assmann, Dr. P. Mostafalu,
Prof. A. Khademhosseini
Harvard-MIT Division of Health Sciences and Technology
Massachusetts Institute of Technology
Cambridge, MA 02139, USA

Prof. N. Annabi, Dr. S. R. Shin, Dr. A. Tamayol, Dr. A. Assmann,
Prof. A. Khademhosseini
Wyss Institute for Biologically Inspired Engineering
Harvard University
Boston, MA 02115, USA

Prof. N. Annabi
Department of Chemical Engineering
Northeastern University
Boston, MA 02115-5000, USA

Dr. A. Assmann
Department of Cardiovascular Surgery
Heinrich Heine University
40225 Düsseldorf, Germany

Prof. J.-Y. Sun
Department of Material Science and Engineering
Seoul National University
Seoul 151-742, South Korea

Prof. S. Mithieux, Prof. A. S. Weiss
Molecular Bioscience
Charles Perkins Centre
Bosch Institute, University of Sydney
Sydney, NSW 2006, Australia

L. Cheung, Prof. X. (S.) Tang
Department of Chemistry
University of Waterloo
Waterloo, Ontario N2L 3G1, Canada

Prof. A. Khademhosseini
Department of Physics
King Abdulaziz University
Jeddah 21569, Saudi Arabia



DOI: 10.1002/adma.201503255

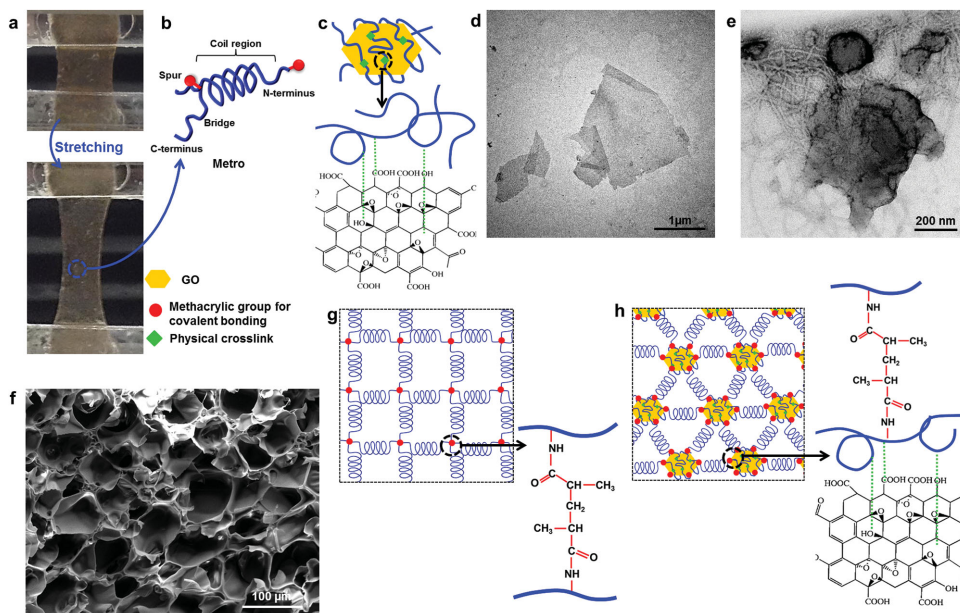


Figure 1. Formation of MeTro/GO hybrid hydrogel. a) Representative images from highly elastic MeTro/GO hydrogel before and after stretching formed by using 1 mg mL^{-1} GO and 10% (w/v) MeTro prepolymer solution. b) Extensible MeTro molecule with an asymmetric coil and a C-terminal cell interactive motif. c) GO particles coated by MeTro solution for the formation of hydrophobic bonding between GO particles and MeTro. HRTEM images from d) GO particles in PBS and e) MeTro-coated GO particles in PBS, showing that tropoelastin fibers covered the GO particles. f) Representative SEM image from a highly porous structure of MeTro/GO hybrid gel. g) UV photocrosslinked MeTro hydrogel network formed by covalently bonding of MeTro molecules during UV crosslinking. h) MeTro/GO hydrogel network created by both covalently bonding due to UV crosslinking and physical bonding between GO particles and MeTro molecules.

Previous studies have attempted to engineer conductive hydrogels through incorporation of nanomaterials such as gold nanowires^[21] and carbon nanotubes (CNTs)^[22] within hydrogel networks made of natural or synthetic polymers. Although the incorporation of these nanomaterials improved the elastic modulus and toughness of the engineered hydrogels, their elasticity was significantly reduced.^[23]

Here, we use GO nanoparticles to form conductive and elastomeric MeTro/GO hybrid hydrogels. GO is utilized due to its flexibility, biocompatibility, and ease of dispersion in aqueous solutions.^[24] Unlike other nanomaterial/hydrogel systems, the incorporation of GO nanoparticles in MeTro enhanced both elasticity and toughness of the engineered hydrogel due to the unique interactions between tropoelastin polymer chains and nanoparticles. Our approach enabled us to tune the mechanical and electrical properties of the engineered bioelastomers. These injectable, light-activated, highly elastic, and conductive hydrogels with their unique mechanical, electrical, and biological properties can be used for various applications such as engineering cardiac tissue constructs, bioactuators, and flexible electronics.

MeTro/GO hybrid hydrogels were formed in a two-step process: (a) dispersion of GO nanoparticles in a 10% (w/v) MeTro prepolymer solution; (b) UV photocrosslinking of the MeTro/GO solution to form a hybrid hydrogel (Figure S1, Supporting Information). Following the crosslinking of the prepolymer solution, a highly elastic MeTro/GO hydrogel with a uniform brown color was obtained (Figure 1a). In addition, high magnification microscopy was conducted to look for large aggregates that may locally change the physical properties of hybrid hydrogels, where

no evidence of nanoparticle aggregation was observed. Both pure MeTro and hybrid hydrogels were easy-to-handle and exhibited high extensibility and stability.

MeTro comprises an asymmetric coil with a protruding “foot” that encompasses the C-terminal cell interaction motif and methacryloyl groups on hydroxyl and lysine residues^[20] (Figure 1b). In particular, this coil region accounts for most of the elasticity of MeTro. Hydrophobic interactions and hydrogen bonding of GO and various polymers has been reported throughout the literature^[25]. Thus, we speculate that hydrophobic and electrostatic interactions were presented between GO particles and MeTro (Figure 1c). A key aim of this study was to homogeneously disperse GO nanoparticles throughout the MeTro solution to form these physical crosslinks while preserving the coil region of the protein to provide elasticity to the matrix.

In our previous study, we showed that GO nanoparticles were successfully dispersed in prepolymer solutions (e.g., gelatin) by coating the particles with a thin layer of gelatin methacryloyl (GelMA) at high temperature ($80 \text{ }^\circ\text{C}$) without using toxic surfactant and sonication process.^[25] We analyzed the GO particles by atomic force microscopy (AFM) to measure their size and thickness.^[25] Height-profile analyses showed that GO sheets have a typical thickness of $(1.6 \pm 0.1 \text{ nm})$ similar to the value reported in a previous study.^[26] The use of high temperature for polymer coating of GO particles is not applicable to MeTro-based prepolymer due to its possible denaturation and coacervation at high temperatures.^[27] To solve this problem, the GO particles were successfully dispersed in MeTro prepolymer solution (1% (w/v)) by sonication at low temperature

(4 °C). The high resolution transmission electron microscope (HRTEM) images showed the morphological differences between bare and MeTro-coated GO nanoparticles, confirming that a thin layer of MeTro polypeptide was uniformly coated on the particle surfaces without particle aggregation (Figure 1d,e). This is in agreement with the pertinent literature, where the ability of proteins to strongly bind onto GO surface due to the electrostatic attraction, hydrophobic interaction, and H-bonding has been reported.^[26] MeTro-coated GO nanoparticles could then easily be dispersed in a 10% (w/v) MeTro prepolymer solution where the initial coating of the particles significantly reduced the particle–particle interactions and prevented their aggregation. The coil regions of MeTro molecules could maintain their unique structures on the surface of GO particles. The large number of the hydrophilic segments of MeTro interact with water and together with the interactions between the hydrophobic segments of its polypeptide chain with GO could effectively coat and separate GO nanoparticles.

The aggregation of particles in a prepolymer solution can introduce weak points in the polymeric network and therefore can reduce the mechanical properties of the resulting hydrogels. To confirm the dispersion of the GO particles in MeTro solution, the overall particle size distributions were assessed using a Zetasizer before and after sonication with MeTro (Figure S2, Supporting Information). The average particle size decreased after coating with MeTro (731.2 ± 71.2 nm) as compared to that of bare particles (1118.5 ± 156.3 nm). This reduction in particle size may be due to cutting or structural damage to GO sheets during the sonication process.

To demonstrate that MeTro/GO hydrogels are useful hybrid materials for tissue engineering applications, it is important to show that enhancing the stiffness of hydrogels through GO incorporation does not affect the favorable characteristics of pure MeTro hydrogel such as porosity and elasticity.^[28] Scanning electron microscopy (SEM) was employed to confirm the porosity and pore morphology of the MeTro/GO hydrogels (Figure 1f). Hybrid hydrogels possessed a highly porous microstructure consisting of ordered polyhedral cells and a uniform pore size (18.3 ± 7.3 μm) comparable to those observed in pure MeTro hydrogels (23.4 ± 5.8 μm).^[12] In addition, the smooth surface of the pore walls in hybrid hydrogel is evidence for the absence of GO aggregates. The swelling ratio measurement also showed that MeTro/GO hydrogels had a lower swelling ratio than pure MeTro hydrogels (Figure S3, Supporting Information). The pure MeTro hydrogels form a network by covalent crosslinks under UV light (Figure 1g). By contrast, in hybrid hydrogels, the matrix is formed by both physical (hydrophobic) bonding between GO particles and MeTro molecules and a large number of covalent bonds in the MeTro matrix (Figure 1h). This combination of physically and covalently crosslinked networks can enhance the toughness, elasticity, and elastic modulus of the hybrid hydrogels in comparison to pure MeTro hydrogel.^[19,29,30]

We first studied the effect of UV exposure time on the elastic modulus of the pure MeTro hydrogel to find the optimum time for photopolymerization of MeTro. The modulus of MeTro hydrogel was about 12.6 ± 0.7 kPa after 6 min of UV exposure with no significant changes after that. The elastic modulus increased to 19.3 ± 0.7 kPa for

hybrid hydrogels containing 1 mg mL⁻¹ GO that were photocrosslinked for 6 min (Figure 2a,b). In addition, the rupture strain was higher for MeTro/GO sample than for pure MeTro ($203 \pm 12\%$ vs. $140 \pm 18\%$). These observations suggest a possible unique interaction between GO nanoparticles and the polymeric network.

In the majority of nanoparticle incorporated hydrogels, the stiffness and toughness of the engineered hybrid is increased through the addition of the nanoparticles.^[22] However, the presence of these nanoparticles can affect the polymer network and reduce the extensibility of the network by creating weak points and nanoscale defects. In our system (explained in Figure 1b) the interactions between MeTro and GO particles appear to enhance both elastic modulus and extensibility. The bridge region of the tropoelastin chain interacts with GO particles through hydrogen bonds and hydrophobic interactions to enhance the mechanical properties of the hybrid networks. These reversible electrostatic and hydrophobic interactions and H-bonding lead to the self-healing and recovery of the hybrid hydrogels.^[31] On the other hand, the coil region of tropoelastin (shown in Figure 1b) preserved the elasticity of the engineered MeTro/GO hydrogels. To qualitatively compare the resilience and recoverability of the engineered hydrogels against torsional stress, the scaffolds were mounted between clamps of an Instron mechanical tester (initial gauge length of 2 cm). Torsion strain was set by controlling the distance between the clamps. While the top clamp was locked, the bottom one was rotated for different numbers of rounds. After each experiment, the elasticity of the hydrogel was checked by rotating back the sample to its original position and measuring the length and width of the sample to evaluate its plastic deformation. The MeTro/GO gel was capable of withstanding dramatic torsional stress without a plastic deformation (Figure 2c), exhibiting extraordinary ductility and flexibility. The hybrid hydrogel did not go under plastic deformation after 23 ± 5 rotations and recovered fully after the rotation; however, pure MeTro gel deformed after the first few rounds and ruptured after 15 ± 4 rotations (Videos S1 and S2, Supporting Information). SEM images of the twisted MeTro/GO sample (Figure 2e) showed that its surface was wrinkled (rumpled) without the formation of cracks. The excellent flexibility and high resistance to torsion in MeTro/GO hydrogel prevented the occurrence of breakage on the surface of the hydrogel. During the torsional deformation, twisted samples experience both compressive and tensile stresses in different directions. Under tension (indicated by blue arrows in Figure 2d), a MeTro chain detaches from a particle surface to relax the applied tension. This MeTro chain can be replaced by another chain belonging to the same or a different polymeric chain to reorganize the network upon compression (indicated by red arrows in Figure 2d). Such continuous reorganization process induces a self-healing characteristic in the network and enhances the energy dissipation. A similar mechanism has been proposed for explaining the resistance of rubber to fracture^[32] and the high elasticity of tough hydrogels containing clay nanoparticles.^[33]

To investigate the resilience of the engineered hydrogels, cyclic tensile tests with a maximum strain of 100% for 1000 cycles were performed. Both MeTro and hybrid gels exhibited negligible hysteresis after 1000 cycles of loading and

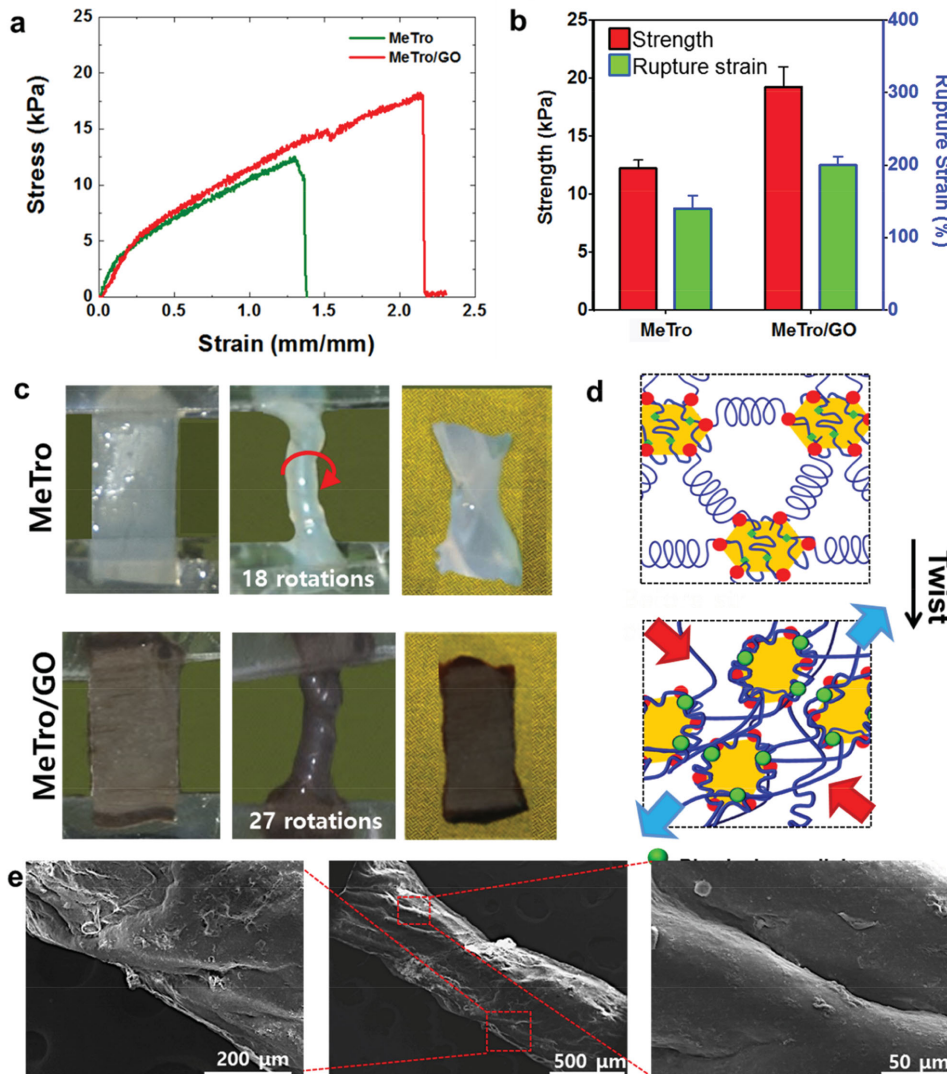


Figure 2. Mechanical characterizations of MeTro/GO hybrid hydrogels under tension and torsion. a) Stress–strain curves of pure MeTro and MeTro/GO hydrogels photocrosslinked after 6 min exposure to UV light (MeTro concentration: 10% (w/v), GO: 1 mg mL⁻¹). b) Rupture strain and ultimate strength for MeTro and MeTro/GO, demonstrating that the addition of GO particles increased both the extensibility and ultimate strength of MeTro hydrogel. c) Images of MeTro and MeTro/GO hydrogels under torsion test (left panel: before the test, middle image: during the test, right image: recovered gel after 10 rounds), significant deformation was observed after 10 times twisting in MeTro gel as compared with no deformation in MeTro/GO gel. d) Schematic illustration of the network structure of the hybrid gel before and after twisting, demonstrating that the hybrid hydrogels undergo both tension (indicated by blue arrows) and compression (indicated by red arrows) during the torsion test. The presence of MeTro fibers will provide high elasticity without hysteresis as the network is stretched; the GO nanoparticles are anchored to the gel networks through physical bonding and act as connectors as the hydrogel network is compressed. These two processes allow for high resilience and minimal deformation of the hybrid network after the torsion test. e) SEM images from the twisted hybrid gel, showing no breakage in the hydrogel structure after twisting.

unloading (Figure 3a). The energy loss for pure MeTro and MeTro/GO hydrogels was calculated based on the area between the loading and unloading curve for cycle 1000. As shown in Figure 3b, MeTro/GO hybrid hydrogels displayed an energy loss of 0.52 kJ m⁻³, which is 34 times higher than pure MeTro (0.01 kJ m⁻³). Both hydrogels maintained a low hysteresis compared with most conventional hydrogels, which exhibit high hysteresis and permanent deformation after unloading.^[30] For example, in a recent study highly stretchable alginate/polyacrylamide hybrid hydrogels showed pronounced hysteresis and permanent deformation.^[19] The higher hysteresis in the

hybrid hydrogels might be due to the continuous formation and rupture of non-covalent bonds, which absorbs more energy in comparison to pure MeTro.

We also compared the fracture toughness of MeTro/GO hybrid hydrogel with pure MeTro gel. We captured time lapsed video images of the single edge notch test for MeTro/GO hydrogel (Figure 3c,d). The frame-by-frame images showed that crack propagation significantly slowed down with the addition of GO particles, providing further evidence of the interactions between GO particles and MeTro. Further, the notched MeTro/GO hybrid hydrogel showed higher ultimate strain

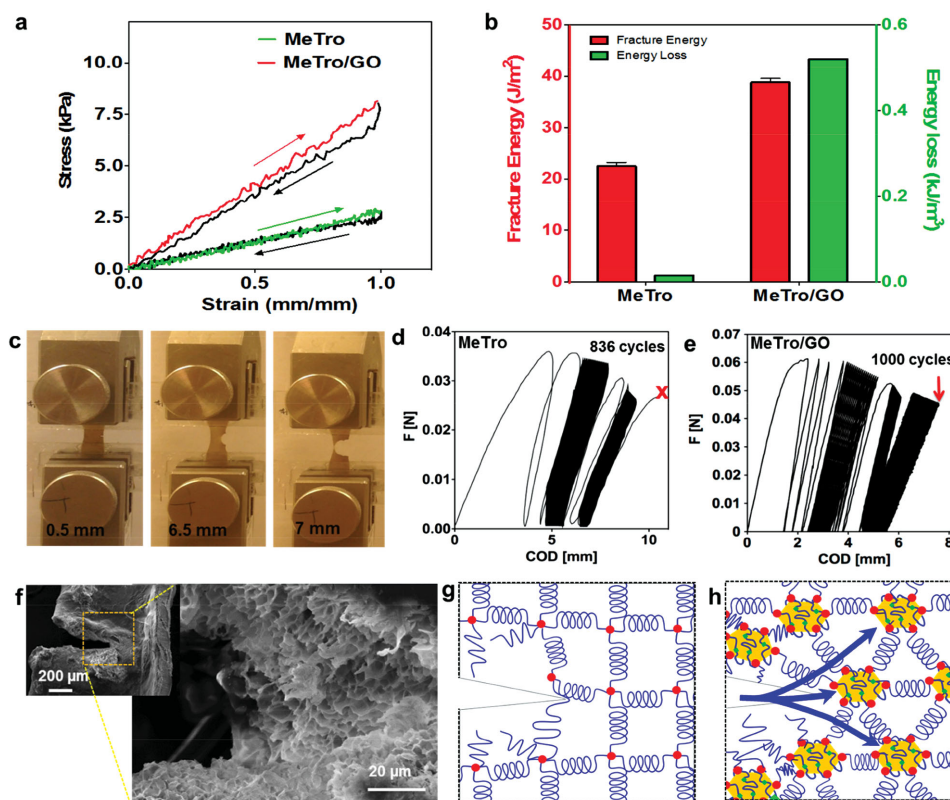


Figure 3. Cyclic tensile test and crack test on MeTro/GO hybrid gel (MeTro concentration: 10% (w/v), GO: 1 mg mL⁻¹). a) Stress–strain curves of MeTro and MeTro/GO hydrogels after 1000 cycles of loading and unloading. b) Energy loss and Fracture energy calculated for MeTro/GO and MeTro. c) Images from MeTro/GO hydrogel with crack under tension. F-COD curves for d) MeTro and e) MeTro/GO hydrogels with cracks, demonstrating that MeTro gel broke from the crack point after 836 cycles of loading and unloading but MeTro/GO hybrid hydrogel underwent more than 1000 cycles (limit of the software) without breakage. f) SEM image of MeTro/GO hybrid gel with the crack. g, h) Schematic illustration of the network structure of the gels during the crack test, showing that crack propagated in the MeTro hydrogel but the presence of GO particles could retard a crack propagation in MeTro/GO hybrid gel.

(150%) compared to that of pure MeTro gel (100%) as shown in the fracture curve in Figure S4, Supporting Information. The hybrid hydrogels also showed a maximum fracture energy of $38.8 \pm 0.8 \text{ J m}^{-2}$, which was 1.6-fold higher than pure MeTro hydrogel (Figure 3c).

We also performed a fatigue crack growth test for a single-edge notch on the hydrogel subjected to constant maximum strain rate of 50%. We measured the crack opening displacement (F-COD) as a function of applied force for both hybrid and pure hydrogels (Figure 3e,f). In the hybrid hydrogels, GO particles prevented crack propagation within the hydrogels and the gels did not break even after 1000 cycles of loading and unloading (Video S4, Supporting Information). However, the pure MeTro broke via crack growth after 836 cycles (Video S3, Supporting Information). After the fatigue crack propagation test, the crack region of the MeTro/GO hybrid hydrogel was observed by SEM (Figure 3f). The hybrid hydrogels still possessed a highly porous microstructures consisting of ordered polyhedral cells and a uniform pore size on the root of notch.

These results provide insight into the mechanisms of deformation and energy dissipation in our highly elastic and tough hydrogels. The elasticity and energy dissipation of MeTro depend

on the interactions between water molecules and hydrophobic domains in tropoelastin. However, when a cracked MeTro hydrogel is stretched, crack propagation can affect the polymer network (Figure 3g). The pure MeTro gel is more notch-sensitive because energy is dissipated over a highly localized region with only a small fraction of the chains in the network participating in energy dissipation. However, in the hybrid gel, the number of chains that participate in energy dissipation is dramatically increased. In addition, GO particles have a high elastic modulus and have been used as reinforcing agents to create porous hydrogels with tunable mechanical properties.^[25] Therefore, when a notched hybrid hydrogel is stretched, the propagation of notch is stopped by the GO particles in hybrid hydrogel (Figure 3h). This was likely the result of the efficient energy transfer between the nanoparticles and MeTro networks, due to their direct coupling, that led to homogeneously distributed GO particles in a large zone being subjected to stress. The load sharing of the MeTro networks and nanoparticles might also have been achieved by entanglements of the MeTro chain on the surface of GO, and by possible covalent crosslinks formed between the acrylic groups on MeTro matrix and MeTro-coated GO particles. Therefore, the incorporation of homogeneously distributed GOs in the macroporous MeTro hydrogel yielded an increase in toughness

due to high densities of physical and covalent crosslinks on the surface of GO particles.

To investigate the effect of nanoparticles on the local and global conductivity of the hybrid hydrogels, a thin layer ($<5\ \mu\text{m}$) of MeTro and MeTro/GO samples were spin-coated on indium tin oxide (ITO) glass slides. In addition, since reduced GO (rGO) offers a higher electrical conductivity in comparison to GO, we created hybrid samples containing rGO instead of GO, for applications where tuning electrical properties is the main target. Conductive AFM analysis was carried out to determine the morphology and local electrical conductance of the samples. As shown in **Figure 4a**, MeTro samples showed a uniform topography, while the samples containing GO and rGO showed uneven surface topography, which was due to the presence of nanoparticles on the surfaces of the hydrogels. Simultaneously, the electrical current passing through the sample was measured by applying a voltage bias in the range of -1 to 1 V. We noticed a few locations where detectable currents passed through the hybrid samples and these locations coincided with the peaks on the surface topography plots. These observations suggest that the incorporated nanoparticles allow electron transfer through the thickness of the sample, while MeTro acted as an electrical insulator. Similar observation was reported for a hybrid alginate/gold nanowire sheet.^[21] Another interesting observation was that the current peaks were more pronounced in samples containing rGO, which was expected, as rGO is more electrically conductive than GO.

We also measured the overall film impedance of pristine MeTro and hybrid hydrogels (**Figure 4b**). The samples were sandwiched between two gold glass slides and AC bias was applied in the range of 1 Hz to 1 kHz. We found that at lower frequencies, which resembled the electrophysiological activity of muscular tissue, the hybrid hydrogels offered lower impedance. Similar to the conductive AFM data, the samples containing rGO had the lowest impedance over the entire frequency range.

A key advantage of the engineered electrically conductive hybrid hydrogel is its capacity for conducting electrical current through biological samples. To assess this phenomenon, abdominal muscle tissues were explanted from rats, cut into square pieces (10×10 mm), and placed in an electrically insulated PDMS mold $\approx 1000\ \mu\text{m}$ apart. Pure MeTro or hybrid hydrogels were then injected in the gap between the tissues and then photocrosslinked as described previously (**Figure 4c**). The hydrogel connected the pieces together and acted as a glue (**Figure 4d**). We then connected each muscle piece to an electrode and applied a DC electrical voltage to the tissues. The beating or contraction of the muscles was checked and the applied voltage was increased until the muscles contracted (**Figure 4e** and **Video S5**, Supporting Information). We observed a lower threshold for muscular tissue connected with hybrid hydrogels compared to the tissues linked with pure MeTro gel. In addition, the electrical threshold for muscular stimulation was lower when MeTro/rGO was used as a connector between tissues compared to MeTro/GO, confirming the higher conductivity of hybrid hydrogels containing rGO. Due to the large thickness of the applied hydrogel layer, this observation suggests a positive role of the nanoparticles on the global conductivity of the hybrid materials.

Normal function of muscular cells and engineered tissues requires a scaffold that can mimic in vivo mechanical and electrical properties. Here, we used the engineered hybrid hydrogel to assess the growth and function of neonatal rat cardiomyocytes (CMs) and cardiac fibroblasts (CFs). We found that both pure and hybrid hydrogels supported the attachment and growth of CFs (**Figure S5**, Supporting Information) and CMs (**Figure S6**, Supporting Information). CF spreading and proliferation was promoted in hybrid hydrogels containing higher concentration of GO (**Figure S5**, Supporting Information). Similarly, higher number of CMs attached to hybrid hydrogels on day 1 and the surfaces of hydrogels were completely covered with CMs by day 7 of culture as shown by SEM and F-actin stained images (**Figure S6a,b**, Supporting Information). After 1 day of culture, the average cell area of $559 \pm 57\ \mu\text{m}^2$ on MeTro/GO ($2\ \text{mg mL}^{-1}$) was twice that of pure MeTro ($315 \pm 40\ \mu\text{m}^2$) (**Figure 4g**). The activity of CMs cultured on pure and hybrid hydrogels did not drop over 7 day of culture, confirming the cytocompatibility of the hybrid hydrogels (**Figure S6c**, Supporting Information). In our previous studies, GO particles showed adsorption of large amount of proteins (e.g., fetal bovine serum and growth factor) onto their nanostructures by noncovalent interactions which resulted in an increased cell attachment and proliferation.^[34] Therefore, we expect that these characteristics of hybrid materials should support better cell behavior than the neat hydrogel. These observations are in line with the previous studies reporting strong cellular adhesion and proliferation on nanomaterials incorporated ECM-based hydrogels.^[22,25]

Immunohistochemical analyses demonstrated the maturation of CMs cultured on both pure and hybrid hydrogels after 7 day of culture (**Figure 4f** and **Figure S7**, Supporting Information). Expression of troponin I, sarcomeric α -actinin, and connexin-43 was higher on MeTro/GO containing $2\ \text{mg mL}^{-1}$ GO than pure MeTro and hybrid gel containing $1\ \text{mg mL}^{-1}$ GO as shown in **Figure 4f** and **Figure S7a,b**, Supporting Information. In addition, sarcomeric α -actinin staining on samples showed that the cells had developed well-aligned sarcomeric structures on hybrid hydrogels containing $2\ \text{mg mL}^{-1}$ GO (**Figure S7b**, Supporting Information), which resembled those of native adult rat ventricular myocardium. Quantification of sarcomere alignment demonstrated that GO nanoparticles improved the alignment of the expressed sarcomeres. We also characterized the beating behavior of CMs seeded on the engineered hydrogels (**Figure S8**, Supporting Information). CMs seeded on MeTro/GO hybrid gels containing higher concentration of GO displayed stronger and synchronized contractions by as early as day 3 that contrasted with pure MeTro hydrogels (**Videos S6** and **S7**, Supporting Information). The beat frequency, quantified between days 3 and 12, varied between 20 – $85\ \text{beats min}^{-1}$ depending on GO concentration. The highest beating frequency of CMs was observed on day 7 on MeTro/GO hydrogels containing $2\ \text{mg mL}^{-1}$ GO. In addition, for all the samples, beating frequency decreased from day 6 to day 12 of culture.

To study the effect of GO nanoparticle on excitation threshold, we applied square-wave pulse electrical stimulation (less than 15 V) with relatively short duration according to a previous protocol.^[11] Cells contracted in synchrony in response to the applied stimulation on all samples, and could be paced using

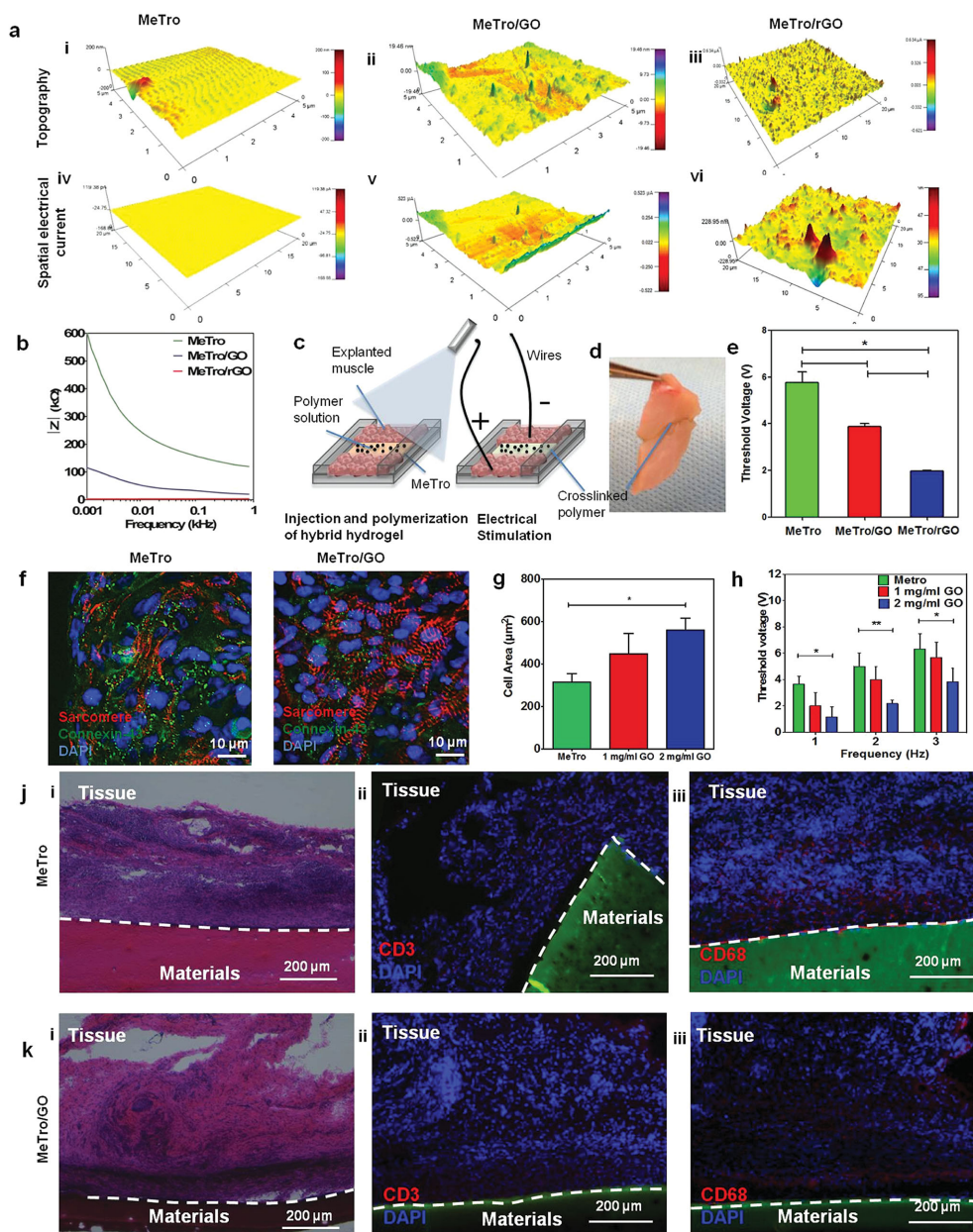


Figure 4. Electrical and biological characterizations of engineered hybrid hydrogels. a) Spatial topography and conductivity of (i, iv) pure MeTro, (ii, v) MeTro/GO hybrid, and (iii, vi) MeTro/rGO hydrogels, measured by conductive probe atomic force microscopy (C-AFM). Surface topographical mapping shown in (i–iii), demonstrating that the presence of nanoparticles changed the surface topography of the hydrogels. Spatial conductivity of hydrogels presented in iv–vi, showing current spikes at the location of nanoparticles in hybrid gels. b) Overall impedance of pure MeTro and hybrid hydrogels, showing lower electrical resistance for hybrid hydrogels. c) The schematic illustration of ex vivo setup used for measuring excitation threshold of muscle tissue. Two pieces of rat abdominal muscles were placed in closed proximity (1 mm apart) and the hydrogels were injected and photopolymerized between the tissues to connect them together. An electrical potential was applied on tissues by using an electrical function generator and the minimum voltage to induce muscle contraction was measured and reported as excitation threshold. d) Representative image of two pieces of muscle connected with MeTro/GO hybrid gel. e) Excitation threshold of muscle tissue connected by pure MeTro and hybrid gels, demonstrating that, MeTro/rGO hybrid gels gave rise to the lowest excitation threshold, which was due to the highest conductivity of the MeTro/rGO hybrid gels. f) Immunostaining for the expression of sarcomeric α -actinin (red)/connexin-43 (green)/nuclei (blue) on CM-seeded pure MeTro and hybrid gels on day 7 of culture. g) Cell spreading, defined as the area of cell clusters divided by the number of the cells within those cluster, on MeTro, MeTro/GO (1 mg mL⁻¹ GO), and MeTro/GO (2 mg mL⁻¹ GO) on day 7 of culture, demonstrating higher cell spreading on MeTro/GO samples compared to MeTro. h) Excitation threshold of cardiac tissues on MeTro (green), MeTro/GO (1 mg mL⁻¹ GO) (red), and MeTro/GO (2 mg mL⁻¹ GO) (blue) at various frequencies. j, k) Histology and immunohistology images of pure MeTro and MeTro/GO hydrogels 28 days after implantation in the subcutaneous tissue of a rat. H&E images are shown in (i) and immunohistology images of gels stained for CD3 (T-lymphocytes, in red) and CD68 (macrophages, red) are shown in (ii) and (iii), respectively. The immunohistology images showed that there were no T-lymphocytes present in any of the explanted samples, confirming the biocompatibility of both the pure and hybrid gels. Error bars represent the SD of measurements performed on five samples ($*p < 0.05$, $**p < 0.01$).

50 ms pulses of electrical stimulation up to 3 Hz (Video S8, Supporting Information). The excitation threshold of CMs cultured on hybrid and pristine hydrogels were characterized by applying electrical pulses between two carbon electrodes. The excitation threshold which is the minimum voltage required to induce synchronous beating at different frequencies (e.g., 0.5, 1, 2, 3 Hz), was determined for each condition. The excitation threshold was lower on hybrid hydrogels in comparison to pure hydrogels at different frequencies (Figure 4h). For example, at an applied frequency of 2 Hz, the excitation threshold was approximately 2.3-fold lower for the hybrid gel with 2 mg mL⁻¹ GO as compared to pure MeTro gel (2.2 V vs 5 V) (**P* < 0.05). These *in vitro* studies together demonstrated that the incorporation of GO particles within the MeTro hydrogel could promote CM growth, proliferation, spreading, phenotype and synchronous beating of CMs. Similar behaviors were observed for CM seeded on GelMA/GO hydrogels^[25] and alginate/gold nanowire hydrogels.^[21] We believe that the presence of conductive nanoparticles enhances local and nanoscale electrical conductivity and induces cell–cell signaling, which in turn promotes cellular function.

In order to test the *in vivo* biocompatibility of pure and hybrid hydrogels, samples were subcutaneously implanted in rats. Hematoxylin/eosin (H&E) staining after 28 days *in vivo* showed good integration of the samples in the host environment, whereas cellular invasion into the hydrogels was not observed within the short follow-up period (Figure 4j(i),k(i)). Immunostaining against the lymphocyte marker CD3 did not result in substantially positive signals in any group (Figure 4j(ii),k(ii)), while there was moderate macrophage infiltration in the subcutaneous tissue around the implants of both groups as indicated by positive staining for CD68 (Figure 4j(iii),k(iii)). Similar observations were seen in histological and immunostaining images from the samples explanted 3 days after implantation (Figure S9, Supporting Information).

Before being considered as conductive implant material, toxic and immunogenic effects of the hydrogels have to be excluded. In the present project, biocompatibility testing in a subcutaneous rat model revealed that MeTro as well as MeTro/GO hydrogels did not induce relevant local inflammation when used as implants. To the best of our knowledge, this is the first report on such an *in vivo* analysis of MeTro-based hydrogels. Moreover, significant biodegradation *in vivo* does not occur within the first 4 weeks. If these hydrogels are used as conductive implants, their slow degradation is beneficial, since the electrical functionality and structural integrity of the grafts should be maintained as long as regenerative tissue has not replaced the implanted scaffold. However, further investigation on the long-term fate of the implanted material seems to be warranted.

In summary, we have developed human protein based hybrid hydrogels that offer a combination of elasticity, electrical conductivity, and bioactivity. The hybrid materials were formed by incorporating GO nanoparticles into a highly elastic MeTro-based hydrogel. Different from other nanohybrid systems, the incorporation of nanoparticles improved both toughness and elasticity of the engineered hydrogels. This was due to a combination of covalent bonds between polymeric chains and hydrophobic, electrostatic interactions, and hydrogen-bonds between the polymer chains and GO nanoparticles. Thus,

the engineered hybrid materials showed a superior resilience against cyclic tensile and torsional forces. In addition, the developed hybrid material allowed conductance of electrical current and were successfully used for connecting pieces of explanted abdominal muscles. The hybrid hydrogels allowed electrical current to pass through the defective area. These conductive elastomers also supported CM growth and function and enhanced their activity and maturation in comparison to pure MeTro hydrogels. The engineered hybrids were also found to be biocompatible by triggering a low to moderate inflammatory response after implantation in rats. The synthesized conductive and elastomeric hydrogels with their tunable electrical and mechanical properties can be used for a range of tissue engineering and regenerative medicine applications.

Experimental Section

Materials: Chemical reagents were purchased from Sigma-Aldrich St. Louis, MO, USA unless mentioned otherwise. MeTro with 44% methacrylation degree was prepared according to procedures explained in our previous studies.^[11,12] Briefly, 15% (v/v) methacrylate anhydride (MA, Sigma) was added to a 10% (w/v) tropoelastin solution (Synthetic Human Elastin without domain 26A, recombinant human tropoelastin isoform SHELdelta26A) in phosphate buffered saline (PBS, Invitrogen). The solution was reacted for 12 h at 4 °C and then diluted and dialyzed using Slide-A-Lyzer MINI, 3.5kDa molecular weight cut-off (MWCO) against water at 4 °C for 48 h. The MeTro prepolymer solution was then filtered and lyophilized for further use. The methacryloyl modification of tropoelastin was confirmed by performing ¹H NMR analysis as previously described.^[12]

Preparation of MeTro/GO Hybrid Hydrogel: To form MeTro/GO hydrogels, GO nanoparticles were first dispersed in MeTro prepolymer solution in PBS. GO was obtained from graphite following modified Hummer's method. To obtain homogenous dispersion of nanoparticles in MeTro, GO particles were first coated with MeTro by sonication (VCX 400, 80 W, 2 s on and 1 s off) of a 1% (w/v) MeTro solution containing 5 mg mL⁻¹ GO for 1 h in ice bath. A selected amount of this solution was then added to a MeTro solution (10% w/v) containing 0.5% photoinitiator, 2-hydroxy-1-(4-(hydroxyethoxy) phenyl)-2-methyl-1-propanone (Irgacure 2959, CIBA Chemicals), to prepare prepolymer solutions for gelation, with a final concentration of GO at 0, 1, and 2 mg mL⁻¹. To prepare hydrogel film, 10 μL prepolymer solution was placed between two glass coverslips that were separated by a 150 μm spacer and exposed to 6.9 mW cm⁻² UV light (360–480 nm) for 6 min (optimized UV exposure time to fully polymerized the hydrogels). To confirm the dispersion of the GOs in MeTro solution, the overall particle size distribution of GOs was measured before and after mixing with MeTro (1 mg mL⁻¹) by a Zetasizer. High resolution transmission electron microscope (HRTEM) images (Tecna 12, FEI, The Netherlands) were acquired using a charge coupled detector (CCD) camera to observe the morphology of MeTro coated GO particles. All sample solutions were loaded onto holey carbon film-supported grids with negative staining (Uranyl acetate).

For conductivity experiments, rGO particles were used. To make rGO, ascorbic acid (L-Ascorbic acid 2-phosphate sesquimagnesium salt hydrate, Sigma-Aldrich, USA) was dissolved in 15 mL of the GO solution. Then, the mixture was placed in a sonicator (Crest Ultrasonics, Model No 275DA, USA) for 60 min. Afterward, the solution was kept in the oven at 80 °C for 48 h in order to accelerate the reduction process. Then, the solution was dialyzed using dialysis membrane tubing with 12–14 kDa MWCO against distilled water for 5 days at room temperature. The rGO solution in PBS was then mixed with MeTro prepolymer solution and subsequently photopolymerized to form MeTro/rGO hydrogels, using similar procedure explained above for the fabrication of MeTro/GO

gels. The methods used to characterize the physical properties of the engineered hydrogels can be found in the Supporting Information.

Supporting Information

Supporting Information is available from the Wiley Online Library or from the author.

Acknowledgements

N.A. and S.R.S. contributed equally to this work. A.A. acknowledges postdoctoral funding from the German Heart Foundation, Frankfurt, Germany (S/04/12). A.K. acknowledges funding from the National Science Foundation (EFRI-1240443), ONR PECASE Award, IMMODGEL (602694), and the National Institutes of Health (EB012597, AR057837, DE021468, HL099073, AI105024, and AR063745). ASW acknowledges funding from the NIH (EB014283), the Australian Research Council, and National Health and Medical Research Council (NHMRC). N.A. acknowledges a CJ Martin Fellowship from the NHMRC. The Animal Experimentation Protocol used to obtain the results presented in this study was approved by the Harvard Medical Area Standing Committee on Animals on 10.11.2013.

Received: July 6, 2015

Revised: July 30, 2015

Published online: November 9, 2015

- [1] a) Y. Wang, G. A. Ameer, B. J. Sheppard, R. Langer, *Nat. Biotechnol.* **2002**, *20*, 602; b) G. C. Engelmayr, M. Cheng, C. J. Bettinger, J. T. Borenstein, R. Langer, L. E. Freed, *Nat. Mater.* **2008**, *7*, 1003.
- [2] Q. Chen, S. Liang, G. A. Thouas, *Prog. Polym. Sci.* **2013**, *38*, 584.
- [3] a) F. Borcan, C. M. Soica, S. Ganta, M. M. Amiji, C. A. Dehelean, M. F. Munteanu, *Chem. Cent. J.* **2012**, *6*, 87; b) S. M. Mithieux, S. G. Wise, A. S. Weiss, *Adv. Drug Delivery Rev.* **2013**, *65*, 421.
- [4] a) O. Chaudhuri, L. Gu, M. Darnell, D. Klumpers, S. A. Bencherif, J. C. Weaver, N. Huebsch, D. J. Mooney, *Nat. Commun.* **2015**, *6*; b) K.-H. Nam, N. Jamilpour, E. Mfoumou, F.-Y. Wang, D. D. Zhang, P. K. Wong, *Sci. Rep.* **2014**, *4*.
- [5] a) A. H. Najafabadi, A. Tamayol, N. Annabi, M. Ochoa, P. Mostafalu, M. Akbari, M. Nikkhah, R. Rahimi, M. R. Dokmeci, S. Sonkusale, B. Ziaie, A. Khademhosseini, *Adv. Mater.* **2014**, *26*, 5823; b) R. Libanori, R. M. Erb, A. Reiser, H. Le Ferrand, M. J. Süess, R. Spolenak, A. R. Studart, *Nat. Commun.* **2012**, *3*, 1265; c) M. S. White, M. Kaltenbrunner, E.D. Glowacki, K. Gutnichenko, G. Kettlgruber, I. Graz, S. Aazou, C. Ulbricht, D. A. M. Egbe, M. C. Miron, Z. Major, M. C. Scharber, T. Sekitani, T. Someya, S. Bauer, N. S. Sariciftci, *Nat. Photonics* **2013**, *7*, 811.
- [6] a) Z. Pei, Y. Yang, Q. Chen, E. M. Terentjev, Y. Wei, Y. Ji, *Nat. Mater.* **2014**, *13*, 36; b) P. Fratzl, F. G. Barth, *Nature* **2009**, *462*, 442.
- [7] R.-H. Kim, D.-H. Kim, J. Xiao, B. H. Kim, S.-I. Park, B. Panilaitis, R. Ghaffari, J. Yao, M. Li, Z. Liu, V. Malyarchuk, D. G. Kim, A.-P. Le, R. G. Nuzzo, D. L. Kaplan, F. G. Omenetto, Y. Huang, Z. Kang, J. A. Rogers, *Nat. Mater.* **2010**, *9*, 929.
- [8] a) K. L. Fujimoto, K. Tobita, J. Guan, R. Hashizume, K. Takanari, C. M. Alfieri, K. E. Yutzey, W. R. Wagner, *J. Card. Failure* **2012**, *18*, 585; b) S. A. Guelcher, K. M. Gallagher, J. E. Didier, D. B. Klinedinst, J. S. Doctor, A. S. Goldstein, G. L. Wilkes, E. J. Beckman, J. O. Hollinger, *Acta Biomater.* **2005**, *1*, 471.
- [9] a) D. W. Lim, D. L. Nettles, L. A. Setton, A. Chilkoti, *Biomacromolecules* **2007**, *8*, 1463; b) S. R. MacEwan, A. Chilkoti, *Biopolymers* **2010**, *94*, 60.
- [10] a) S. M. Mithieux, J. E. Rasko, A. S. Weiss, *Biomaterials* **2004**, *25*, 4921; b) J. Rnjak, Z. Li, P. K. M. Maitz, S. G. Wise, A. S. Weiss, *Biomaterials* **2009**, *30*, 6469.
- [11] N. Annabi, K. Tsang, S. M. Mithieux, M. Nikkhah, A. Ameri, A. Khademhosseini, A. S. Weiss, *Adv. Funct. Mater.* **2013**, *23*, 4950.
- [12] N. Annabi, S. M. Mithieux, P. Zorlutuna, G. Camci-Unal, A. S. Weiss, A. Khademhosseini, *Biomaterials* **2013**, *34*, 5496.
- [13] N. Annabi, S. M. Mithieux, E. A. Boughton, A. J. Ruys, A. S. Weiss, F. Dehghani, *Biomaterials* **2009**, *30*, 4550.
- [14] N. Annabi, S. M. Mithieux, A. S. Weiss, F. Dehghani, *Biomaterials* **2009**, *30*, 1.
- [15] a) K. Haraguchi, T. Takehisa, *Adv. Mater.* **2002**, *14*, 1120; b) J. Djonlagic, D. Žugic, Z. Petrovic, *J. Appl. Polym. Sci.* **2012**, *124*, 3024.
- [16] Y. Okumura, K. Ito, *Adv. Mater.* **2001**, *13*, 485.
- [17] J. P. Gong, *Soft Matter* **2010**, *6*, 2583.
- [18] M. A. Haque, T. Kurokawa, G. Kamita, J. P. Gong, *Macromolecules* **2011**, *44*, 8916.
- [19] J.-Y. Sun, X. Zhao, W. R. K. Illeperuma, O. Chaudhuri, K. H. Oh, D. J. Mooney, J. J. Vlassak, Z. Suo, *Nature* **2012**, *489*, 133.
- [20] C. Baldock, A. F. Oberhauser, L. Ma, D. Lammie, V. Siegler, S. M. Mithieux, Y. Tu, J. Y. Chow, F. Suleman, M. Malfois, S. Rogers, L. Guo, T. C. Irving, T. J. Wess, A. S. Weiss, *Proc. Natl. Acad. Sci. USA* **2011**, *108*, 4322.
- [21] T. Dvir, B. P. Timko, M. D. Brigham, S. R. Naik, S. S. Karajanagi, O. Levy, H. Jin, K. K. Parker, R. Langer, D. S. Kohane, *Nat. Nanotechnol.* **2011**, *6*, 720.
- [22] S. R. Shin, H. Bae, J. M. Cha, J. Y. Mun, Y. C. Chen, H. Tekin, H. Shin, S. Farschi, M. R. Dokmeci, S. Tang, A. Khademhosseini, *ACS Nano* **2012**, *6*, 362.
- [23] a) S. F. Wang, L. Shen, W. D. Zhang, Y. J. Tong, *Biomacromolecules* **2005**, *6*, 3067; b) C. Lynam, S. E. Moulton, G. G. Wallace, *Adv. Mater.* **2007**, *19*, 5; c) S. Araby, Q. Meng, L. Zhang, I. Zaman, P. Majewski, J. Ma, *Nanotechnology* **2015**, *26*, 112001.
- [24] a) X. Zhang, J. Yin, C. Peng, W. Hu, Z. Zhu, W. Li, C. Fan, Q. Huang, *Carbon* **2011**, *49*, 986; b) Y. Chang, S.-T. Yang, J.-H. Liu, E. Dong, Y. Wang, A. Cao, Y. Liu, H. Wang, *Toxicol. Lett.* **2011**, *200*, 201; c) X. Sun, Z. Liu, K. Welscher, J. Robinson, A. Goodwin, S. Zaric, H. Dai, *Nano Res.* **2008**, *1*, 203.
- [25] S. R. Shin, B. Aghaei-Ghareh-Bolagh, T. T. Dang, S. N. Topkaya, X. Gao, S. Y. Yang, S. M. Jung, J. H. Oh, M. R. Dokmeci, X. Tang, A. Khademhosseini, *Adv. Mater.* **2013**, *25*, 6385.
- [26] Q. Mu, W. Liu, Y. Xing, H. Zhou, Z. Li, Y. Zhang, L. Ji, F. Wang, Z. Si, B. Zhang, B. Yan, *J. Phys. Chem. C* **2008**, *112*, 3300.
- [27] B. Vrhovski, S. Jensen, A. S. Weiss, *Eur. J. Biochem.* **1997**, *250*, 92.
- [28] a) M. P. Lutolf, P. M. Gilbert, H. M. Blau, *Nature* **2009**, *462*, 433; b) J. W. Nichol, S. T. Koshy, H. Bae, C. M. Hwang, S. Yamanlar, A. Khademhosseini, *Biomaterials* **2010**, *31*, 5536.
- [29] A. B. Ihsan, T. L. Sun, S. Kuroda, M. A. Haque, T. Kurokawa, T. Nakajima, J. P. Gong, *J. Mater. Chem. B* **2013**, *1*, 8.
- [30] a) M. Tan, T. Zhao, H. Huang, G. Mingyu, *Polym. Chem.* **2013**, *4*, 6; b) T. L. Sun, T. Kurokawa, S. Kuroda, A. B. Ihsan, T. Akasaki, K. Sato, M. A. Haque, T. Nakajima, J. P. Gong, *Nat. Mater.* **2013**, *12*, 932; c) Y. Yue, T. Kurokawa, M. A. Haque, T. Nakajima, T. Nonoyama, X. Li, I. Kajiwara, J. P. Gong, *Nat. Commun.* **2014**, *5*, 4659.
- [31] a) Y. Fang, C. F. Wang, Z. H. Zhang, H. Shao, S. Chen, *Sci. Rep.* **2013**, *3*, 2811; b) A. Phadke, C. Zhang, B. Arman, C. C. Hsu, R. A. Mashelkar, A. K. Lele, M. J. Tauber, G. Arya, S. Varghese, *Proc. Natl. Acad. Sci. USA* **2012**, *109*, 4383; c) D. C. Tuncaboylu, M. Sari, W. Oppermann, O. Okay, *Macromolecules* **2011**, *44*, 9.
- [32] G. J. Lake, A. G. Thomas, *Proc. R. Soc. London, Ser. A* **1967**, *300*, 108.

- [33] a) Q. Wang, J. L. Mynar, M. Yoshida, E. Lee, M. Lee, K. Okuro, K. Kinbara, T. Aida, *Nature* **2010**, 463, 339; b) K. Haraguchi, K. Uyama, H. Tanimoto, *Macromol. Rapid Commun.* **2011**, 32, 1253; c) L. Carlsson, S. Rose, D. Hourdet, A. Marcellan, *Soft Matter* **2010**, 6, 3619; d) A. K. Gaharwar, C. P. Rivera, C.-J. Wu, G. Schmidt, *Acta Biomater.* **2011**, 7, 4139.
- [34] X. Shi, H. Chang, S. Chen, C. Lai, A. Khademhosseini, *Adv. Funct. Mater.* **2012**, 22, 751.
-